Polarized Soft X-ray Scattering Reveals Chain Orientation within Nanoscale Polymer Domains

Joshua H. Litofsky,[†] Youngmin Lee,[†] Melissa P. Aplan,[†] Brooke Kuei,[‡] Alexander Hexemer,[∥] Cheng Wang,[∥] Qing Wang,[‡] and Enrique D. Gomez*[,†,‡,§]

[†]Department of Chemical Engineering, [‡]Department of Materials Science and Engineering, and [§]Materials Research Institute, The Pennsylvania State University, University Park, Pennsylvania 16802, United States

[∥]Advanced Light Source, Lawrence Berkeley National Laboratory, Berkeley, California 94530, United States

ABSTRACT: Fully conjugated donor−acceptor block copolymers can serve as the active layer in organic photovoltaics and other organic electronic devices. Self-assembly into periodic domains and crystallization of the constituent blocks are crucial to enable control of the multiscale structure and consequently electronic properties. Resonant soft X-ray scattering (RSoXS) is an invaluable tool to characterize such materials, where tuning the X-ray energy and polarization reveals molecular orientation and domain spacing. Here, anisotropic soft X-ray scattering data reveal the type and degree of orientation within conjugated block copolymers composed of poly(3-hexylthiophene-2,5-diyl) and various push−pull copolymers. The maximum anisotropy is observed at the scattering vector corresponding to the spacing between block copolymer domains, which scales with the end-to-end distance of the blocks, as expected. Furthermore, the anisotropy in RSoXS data reveals that the crystalline P3HT blocks orient, on average, parallel or nearly parallel to the block copolymer interface; the average tilt angle between P3HT chains and domain interfaces can be extracted from the dependence of the anisotropy with polar angle. We interpret this angle to correspond to the average tilt of rings in the unit cell, potentially within a chiral mesostructure. Results are corroborated with scattering calculations based on simple model structures.

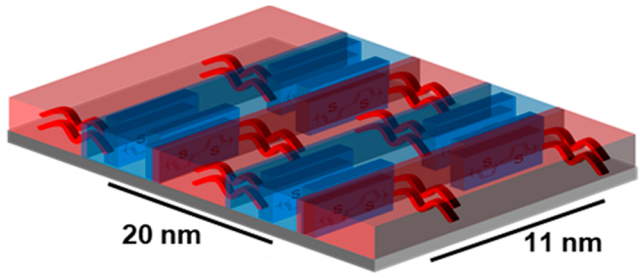

INTRODUCTION

Conjugated polymers used in organic electronics offer a remarkable combination of inherent advantages in flexibility, durability, tunability, ease of fabrication, and performance in electronic devices.[1−5] Frequently, a mixture of two or more components is used, taking advantage of various electronic and structural properties within the active layer to further improve device performance.[6−9] Mixed active layers, while presenting a pathway to increased performance and added functionality, are nonetheless limited by substantial challenges in controlling the nanoscale morphology due to the potential for phase separation.

To address the morphological limitations found in multicomponent blends, self-assembly into ordered structures is warranted. For example, achieving a highly ordered microscale morphology in polymer−polymer and polymer−fullerene blends is difficult and often relies on careful optimization of fabrication and processing conditions. These mixtures produce a partially phase separated and kinetically trapped structure that is seldom optimized for charge generation and overall device performance.[10−12] Thus, a need exists for polymer systems with controllable microstructures. One approach relies on block copolymers composed of two or more covalently bound homopolymers, such that self-assembly leads to periodic nanostructures.[6,13−19]

A challenge with block copolymers is that small density differences between most constituent polymers make microstructure characterization through conventional methods difficult.[14,20,21] Previous studies determined the microstructure of polymer thin films using hard (ca. 10 keV) X-rays to probe molecular packing.[22−24] In particular, grazing incidence small-angle X-ray scattering (GISAXS) and grazing incidence wide-angle X-ray scattering (GIWAXS) provide invaluable information about the long-range order of organic thin films.[25−28] These hard X-ray techniques based on reflection geometries can examine films of varying thickness with high resolution, to the molecular scale (∼1 Å) for GIWAXS and nanoscale (∼1 nm) for GISAXS. Compared to other techniques such as transmission electron microscopy (TEM) and atomic force microscopy (AFM), GISAXS/GIWAXS provides information about the film microstructure over large areas, often with less demanding sample preparation.

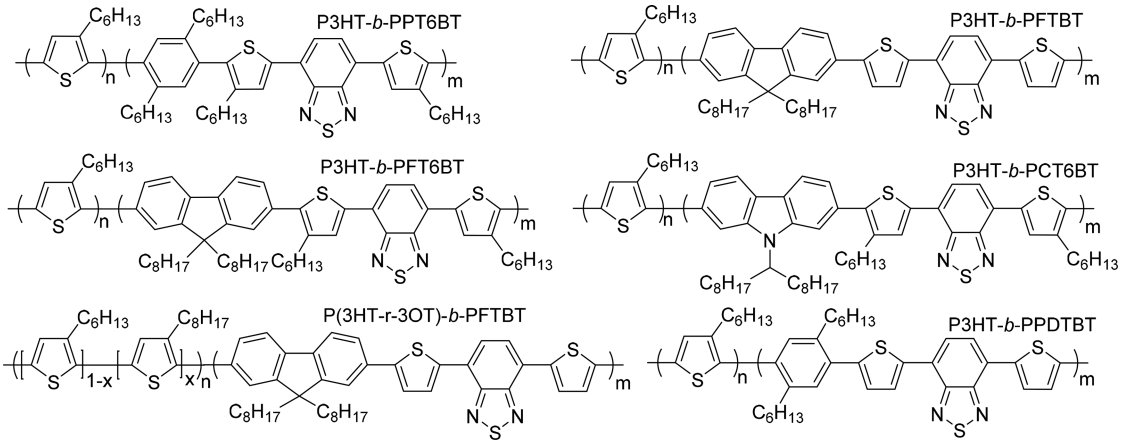

Figure 1. Chemical structures of block copolymers used in this study.

Nevertheless, limitations exist when using high-energy X-ray scattering techniques. For ca. 10 keV X-rays, polymer electron density differences may not be sufficient to garner needed contrast and scattering intensities.[29,30] Additionally, in the hard X-ray regime, scattering cross sections are small enough to require a path length of about 1 mm to maximize scattering, thus preventing studies of polymer thin films in the transmission geometry.[31,32]

One way to address the limitations of hard X-ray scattering experiments is to use lower energy, or "soft", X-rays. By tuning the energy of X-rays to a level in resonance with core electron transition energies in soft materials (200−1000 eV), we can obtain information about long-range order in polymer films. Thus, resonant soft X-ray scattering (RSoXS) takes advantage of differences in the absorbance between multiple phases of soft materials near the carbon, nitrogen, and oxygen absorbance edges.[6,29,32,33] The chemical and elemental sensitivity of RSoXS allows for detailed information about the microscale order of soft materials. At low energies, as differences in X-ray absorption become significant, small differences in optical properties between domains can lead to large contrast from differences in elemental composition, chemical bonding structure, and chain alignment when linearly polarized X-rays are used.[29]

As such, linearly polarized soft X-rays uniquely allow for the study of molecular orientation within nanoscale domains. In RSoXS experiments, an elliptically polarizing undulator controls the polarization of the electric field generated from incoming X-rays.[30] In a sample with multiple domains, such as a block copolymer or a semicrystalline polymer film, differences in the alignment between blocks or phases creates "orientational" contrast. When coupled with chemical contrast, these two contrast mechanisms can provide increased information into the nanoscale structure of the sample.[34−36] Previous work into this contrast mechanism has revealed intriguing information about nanometer-scale molecular orientation of polymers, orientation of polymer chain backbones in adjacent domains, and strength of alignment in semicrystalline polymers.[19,36,37] Furthermore, careful analysis of depolarization of resonant soft X-rays demonstrates sensitivity to local orientation correlations in polymers.[38] Nevertheless, scattering anisotropy is difficult to interpret, and the consequences of linear polarization of soft X-rays on scattering patterns from organic compounds are not yet fully understood.

In this article, we use RSoXS to determine multiple aspects of mesoscale order in a model series of block copolymers (Figure 1). First, simulations of linearly polarized soft X-ray scattering are presented to predict expected results of scattering intensities and anisotropy from idealized morphologies. Simulations are then compared to RSoXS data to reveal the contribution of differences in chain orientation within domains to scattering. Although soft X-ray scattering profiles show some evidence for mesoscale structure, calculating the degree of anisotropy as a function of scattering vector reveals clear peaks associated with microphase separation. Furthermore, examining the dependence of the intensity with polar angle reveals the orientation angle of chains within domains. The combination of scattering simulations and data on model block copolymers demonstrates the sensitivity of RSoXS to chain orientation and provides a route for interpretation of scattering anisotropy.

MATERIALS AND METHODS

Regioregular P3HT (19.6 kg mol^{-1}, 94.8% RR) was purchased from Merck, and all solvents were purchased from Sigma-Aldrich. P3HT-*b*-PFTBT and all other block copolymers were synthesized in-house; block copolymers were synthesized according to previously described procedures.[39−41] All block copolymers are shown in Figure 1.

Samples for RSoXS were prepared using conventional procedures described previously.[6] Silicon wafers were cleaned by soap, followed by 20 min of sonication in acetone and then isopropanol, followed last with 20 min of ultraviolet light ozonation. Poly(3,4-ethylenedioxythiophene):poly(styrenesulfonate), PEDOT:PSS (Clevios P, Heraeus), was spin-coated on the cleaned silicon wafer at 4000 rpm for 120 s at a thickness of about 65 nm. The substrates were then transferred to a nitrogen glovebox, where the P3HT and block copolymer solutions (10 mg/mL in anhydrous chloroform, ≥99% amylenes as stabilizers, Sigma-Aldrich) were stirred at 75 °C overnight in a sealed container prior to casting. These films were removed from the glovebox and floated off the substrate in deionized water; they were consequently picked up with 5 mm × 5 mm silicon frames with a 1 mm × 1 mm, 100 nm thick Si_3N_4 window. Samples were then dried for 3 h under vacuum and annealed on a hot plate at 165 °C in a nitrogen glovebox. RSoXS measurements were done at beamline 11.0.1.2 at the Advanced Light Source at Lawrence Berkeley National Laboratory.[30] A transmission geometry was used under vacuum at the carbon K-edge energy (285 eV) with linearly polarized X-rays; data were corrected for dark current and beam flux. Data were integrated azimuthally and plotted versus scattering vector ($q = 4\pi \sin(\theta/2)/\lambda$, where θ is the scattering angle and λ is the wavelength) and integrated radially and plotted versus polar angle.

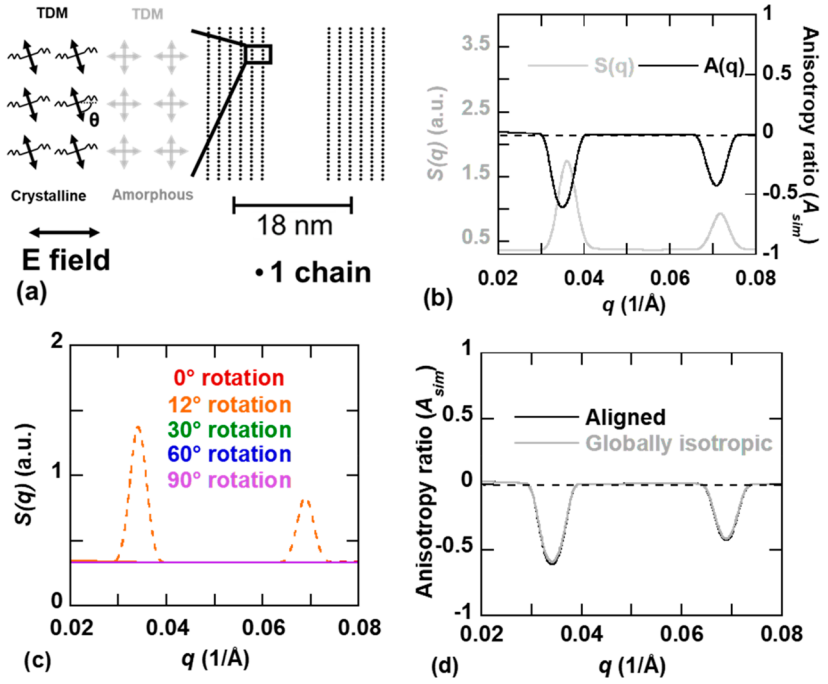

Figure 2. Simulated RSoXS data for a model structure of uniformly oriented neat P3HT crystals. (a) Chain backbones are represented as lines placed 4 Å apart, similar to the P3HT $\pi-\pi$ stacking distance. The chains are uniformly oriented to demonstrate ideal scattering within P3HT. The inset shows TDM arrangement in crystalline and amorphous components, where θ denotes the angle between TDMs and the normal of the crystalline−amorphous interface. (b) RSoXS scattering intensity and anisotropy ratio versus scattering vector q. A primary scattering peak is seen at $q^* = 0.0344$ Å^{-1}, corresponding to crystals with an 18 nm d-spacing. (c) Simulated $S(q)$ versus scattering vector q for the structure shown in (a) with the electric field rotated at different angles and with 0° corresponding to the horizontal direction in (a). Solid lines indicate $S_{\theta+0°}(q)$, and dashed lines indicate $S_{\theta+90°}(q)$. The peak in $S(q)$ is only apparent when the electric field is aligned with the average direction of TDMs (12°). (d) Comparison of the predicted anisotropy ratio from aligned (solid line) and globally isotropic structures (dashed line).

SIMULATIONS OF POLARIZED RSoXS

Given the challenges in interpreting scattering anisotropy in RSoXS data, simulations of scattering from model structures are warranted. A comprehensive effort would incorporate the complex refractive index as a function of energy with the microstructure and local orientations of the transition dipole moments (TDM). Each TDM should be described by an anisotropic scattering tensor. Instead, we aim to capture some of the essential physics of anisotropic soft X-ray scattering with models that are as simple as possible. We start with model structures of semicrystalline polymers with crystalline and amorphous phases and then extend our models to include representations of microphase-separated domains that contain crystalline regions. For simplicity, our models are represented in 2D; for lamellar structures in block copolymers this is sufficient, although proper representations of other morphologies likely require three-dimensional models. We also choose not to represent the energy dependence but instead focus our simulations at energies where scattering is dominated by anisotropic TDMs (e.g., 1s to π^* transitions at 285 eV for carbon).

We consider a model structure of semicrystalline conjugated polymers along the three orthogonal crystallographic directions. When scattering is along the [010] zone axis of a material such as P3HT (i.e., along the π-stacking direction), aligned TDMs are roughly always perpendicular to the X-ray electric field, such that no scattering anisotropy should be apparent. Thus, we ignore this crystal orientation with respect to the X-ray polarization.

Figure 2 shows a model structure of a semicrystalline conjugated polymer along the [001] zone axis with domains of 18 nm that are all uniformly oriented with the $\pi-\pi$ stacking of the polymer backbone. The value for the periodicity was chosen to match experimental results shown in the next section. The X-ray electric field is taken to be polarized horizontally across the structures (along the [100] direction). Figure 2a only shows a small region of our image (three crystals), and the entire image encompasses 20 long crystallites. We set the size of each pixel to be the $\pi-\pi$ stacking distance of 4 Å, as is expected for polymers such as poly(3-hexylthiophene-2,5-diyl) (P3HT). As previously shown, rings can have a tilt angle within crystals,[42] which here we set to 12° from the (100) plane or $\theta = 78°$ from the X-ray electric field; the value for θ is chosen to match the experimental data discussed below. Only chains or portions of chains with fully extended backbones are shown, such that white regions correspond to randomly oriented and amorphous chains (crystalline regions are 50 vol %). We ignore the space between backbones across π-stacks or side chains in crystalline domains, given that scattering for these planes occurs at high q beyond the resolution of RSoXS. The TDM is defined as the in-plane vector perpendicular to the black lines to simulate the π-electron orbitals of conjugated polymers that emanate perpendicular to the chain backbone. As we describe later, the anisotropic scattering from this texture most closely represents our data.

As shown in Figure S1 of the Supporting Information, we also consider scattering along the [100] zone axis. GIWAXS data are commonly interpreted in terms of the predominance of this film texture normal to the substrate.[43−46] Assuming the

backbones are perpendicular to the crystal surface, the anisotropic scattering from this geometry has a maxima at 0° (perpendicular to the X-ray polarization). As discussed below, this does not always describe our experimental data.

The coherence length of the X-ray beam is 10 μm, such that interference between crystals coaligned within this length scale should contribute to scattering. As a simple, toy model of anisotropic scattering, we consider the contributions of chain orientation to the contrast, essentially treating the contributions incoherently. This oversimplification will miss consequences due to depolarization, which have been shown to be significant, especially at high wave vectors.[38] We ignore such effects and simply modulate scattering intensities (essentially through the contrast) by calculating the dot product of the X-ray polarization and the TDM at each pixel; as a consequence, we expect some error in our scattering intensities and degree of anisotropy. Nevertheless, we speculate that the dependences with q and polar angle are accurately represented. Amorphous regions are assigned an isotropic TDM with a value of 1/3 that of aligned chains (corresponding to TDMs that are on average isotropic in 3D). As such, we allow orientation correlations over our model of about 20 crystals (ca. 0.5 μm) to dominate scattering.

Taking the Fourier transform of our model structures converts the real-space structure to the frequency domain.[47,48] The structure factor $S(q)$ is calculated using a simplified Fourier transform. Simulated structures are limited by finite size, reducing the limits of integration. Therefore, the simplified equation for the structure factor in our case is

$$S(q) \propto \sum_{n=1}^{N} e^{iqr_n}\rho(r_n) \tag{1}$$

where N is the number of scattering points (monomers) in our structure and $\rho(r_n)$ is the pair distribution function of black pixels, or the structural data from our model structure.[49] The predicted scattering is shown in Figure 2b as $S(q)$, where the peak at q = 0.035 Å^{-1} corresponds to the 18 nm spacing between crystals.

$S(q)$ is calculated with a Fourier transform across all polar angles. The two-dimensional Fourier transform provides the simulated scattering intensity from −180° to 180°; we use only the scattering intensity at orthogonal angles to probe anisotropy, as shown in Figure S2. The predicted $S(q)$ is maximized in the direction normal to the backbone tilt angle ($S_{\theta+90°}(q)$, where θ = 0 in the direction of the X-ray polarization) and shows peaks associated with the crystal spacing.

By use of eq 1 to generate $S(q)$ in the parallel and perpendicular directions, the anisotropy ratio was calculated as an order parameter to quantify the orientation of chains within the structure via the equation

$$A_{sim}(q) = \frac{S_{\theta+0°}(q) - S_{\theta+90°}(q)}{S_{\theta+0°}(q) + S_{\theta+90°}(q)} \tag{2}$$

where $A_{sim}(q)$ is the simulated anisotropy ratio as a function of q, and $S_{\theta+90°}(q)$ and $S_{\theta+0°}(q)$ are the predicted scattering along the directions perpendicular and parallel to the tilt of the chain backbone, respectively.[36,37,50,51] We can rationalize the relationship between the sign of the anisotropy and the chain orientation within domains by considering that scattering is enhanced in the direction parallel to the TDM. If TDMs are perpendicular (here chain backbones would be parallel) to domain interfaces, scattering is enhanced in the direction of the periodicity of the structure (across the interface). Thus, the anisotropy ratio A ranges from −1 to 1, with A = −1 indicating a perpendicular chain orientation with respect to the domain interface and A = 1 indicating a parallel orientation, as confirmed below by scattering simulations.

In Figure 2b, both the predicted scattering intensity and the anisotropy ratio are shown. A peak in the anisotropy arises at a length scale corresponding to the peak in $S(q)$. The peak is negative as defined in eq 2 because the chains are oriented perpendicular to the interface, and the peak position corresponds to the 18 nm domain spacing. As shown in Figures S3 and S4, the maximum (peak) anisotropy can be limited by disorder in spacing or placement of the chains, disorder in the size of the chains or lamella, and tilting of the chains or lamella.

Our model morphology shown in Figure 2a is aligned over our entire image, such that the predicted anisotropic scattering shown in Figure 2b is not surprising. Within polymer films, lamella and crystalline fibrils are oriented such that the structure is locally anisotropic. Nevertheless, the sample as a whole is globally isotropic, even at length scales corresponding to the X-ray beam size (diameter of about 200−500 μm).[52,53] To calculate the anisotropy ratio for a globally isotropic but locally anisotropic system, we rotate the structure across 0° to 90° while taking the scattering at the θ + 0° and θ + 90° angles and sum the scattering over all rotations. Because of the TDMs being aligned perpendicular to the polymer backbone, chains that are oriented perpendicular to the electric field (and thus have TDMs that are parallel to the electric field) contribute fully to the scattering pattern, whereas chains that are parallel to the electric field do not contribute at all. If we define the angle between the TDM and the electric field of the X-ray beam as α, we can apply a $\cos^2(\alpha)$ weighing function to calculate scattering intensities.[54−56] Using eq 3 to calculate the anisotropy ratio, we see in Figure 2c that the scattering decays quickly as the polar angle deviates from 0°. As a consequence, Figure 2d shows that the anisotropy ratio observed in globally isotropic structures is similar to structures that are aligned over the entire image. The consequence of using linearly polarized X-rays at resonance with transition dipole moments that are locally anisotropic is that the X-ray polarization dictates a sensitivity to the microstructure only in the direction established by TDMs. Thus, if the backbones (and TDMs) are aligned with respect to a domain interface, then scattering from these domains is equivalent, at least in some sense, to scattering from globally aligned samples.

This analysis can be extended to multiphase systems shown in Figure 3 with a crystalline lamellar domain with a spacing of 20 nm in the direction of the X-ray polarization (horizontal); we set this distance to match our experimental data shown in the next section. For simplicity, we ignore defects within crystalline domains. Crystals are oriented such that scattering is along the [001] zone axis, although calculations along the [100] zone axis are possible in a similar manner as that shown for homopolymers in Figure S1. Between the crystalline lamella is an amorphous phase with a spacing of 11 nm along the vertical direction. The empty space still represents chain segments with randomly oriented backbones—now either amorphous chains of the same crystalline polymer or chains from a second component (block) that is amorphous. We can imagine this structure to represent block copolymer lamellae, with crystalline domains spaced 11 nm apart within lamellae

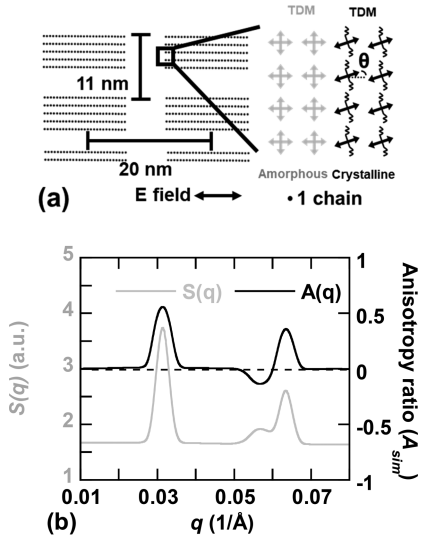

Figure 3. Simulated RSoXS data for one possible arrangement of P3HT crystals in P3HT-*b*-PFTBT. (a) Chain backbones are represented as lines and placed 4 Å apart to simulate P3HT crystals. The inset shows the TDMs of the crystalline components of the structure as compared to the amorphous components. (b) RSoXS scattering intensity and anisotropy ratio versus scattering vector q. Scattering peaks are seen at q = 0.0314 Å^{-1} and at q = 0.057 Å^{-1}, corresponding to "horizontal" periodicity at 20 nm (chains parallel to interface) and "vertical" periodicity at 11 nm (chains perpendicular to interface). The change of sign of the anisotropy ratio reflects the orientation of chain backbones within domains with respect to the interfaces corresponding to the 20 and 11 nm periodicities.

and microphase-separated domains with a periodicity of 20 nm, such that there are two length scales, each associated with a different orientation with respect to the crystal interfaces (amorphous domains are 50 vol % within the crystalline lamellae). The 20 nm domain has chains oriented parallel to the interface while the 11 nm domain has chains oriented perpendicularly.

Calculating the predicted scattering as shown in eq 1 yields a structure factor with peaks at q = 0.031 Å^{-1}, q = 0.057 Å^{-1}, and q = 0.064 Å^{-1}; the first two correspond to the 20 and 11 nm domain sizes, while the third is the second-order reflection of the first peak (Figure 3b). Having established in Figure 2 the equivalence of aligned and globally isotropic morphologies in polarized soft X-ray scattering, we use aligned structures for our $A_{sim}(q)$ calculations from model block copolymer morphologies. The anisotropy shows three peaks at different q values that correspond to peaks in the structure factor; nonetheless, these peaks differ in sign. The low-q peak is positive, corresponding to chains oriented parallel to the crystal interface, while the intermediate-q peak is negative, corresponding to chains oriented perpendicular to the crystal interface. The positive high-q peak at 0.062 Å^{-1} corresponds to the second-order reflection of the first positive peak in $A_{sim}(q)$. As these simple simulations show, the sign of the anisotropy can correspond to the backbone orientation (or direction of the TDM) with respect to domain interfaces. The value of the anisotropy is likely overestimated if crystalline domains are not defect-free, as assumed in our simulations.

RESULTS AND DISCUSSION

Having established the expected scattering and anisotropy from semicrystalline homopolymers and block copolymers, we use P3HT, poly(3-hexylthiophene-2,5-diyl)-*block*-((9,9-dioctylfluorene)-2,7-diyl-*alt*-[4,7-bis(thiophen-5-yl)-2,1,3-benxothiadiazole]-2′,2″-diyl) (P3HT-*b*-PFTBT), and related block copolymer derivatives shown in Figure 1 as model systems to compare experimental data with scattering calculations. P3HT-*b*-PFTBT was chosen because the P3HT block is semicrystalline, the PFTBT block is amorphous, and the block copolymer microphase separates into a lamellar morphology, creating a model morphology for scattering experiments.[33] Films of these materials were spun-cast from chloroform solutions and annealed at 165 °C for 20 min. Figures S5 and S6 show GIWAXS data that confirm crystalline P3HT blocks and amorphous PFTBT; given that liquid crystals will often show a broad diffraction peak, we also speculate that the PFTBT block is isotropic or nearly isotropic.

X-ray absorbance spectra for the constituent polymers of P3HT and PFTBT are shown in Figure 4, with expected scattering contrast shown in Figure S7. At 285 eV, which corresponds to the 1s to π^* core electron transition of carbon−carbon double bonds,[32] the absorbances of P3HT and PFTBT are nearly matched, but significant chemical contrast still exists from dispersive differences between the blocks. The TDM at this energy is anisotropic, and for conjugated polymers these TDMs are aligned perpendicular to the chain backbone.[36,50] Our modeling results shown in Figures 2 and 3 suggest that if the backbones in P3HT-*b*-PFTBT are aligned with respect to a domain interface, then RSoXS scattering will be anisotropic. Thus, near 285 eV, soft X-ray scattering contrast can be dominated from the differences between domains in the net chain orientation (net orientation within each domain),

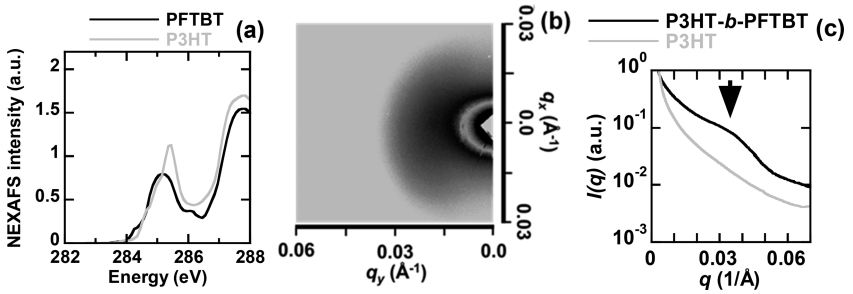

Figure 4. (a) NEXAFS spectra of P3HT and PFTBT films obtained in a transmission geometry, presented to demonstrate the large optical differences between P3HT and PFTBT at resonance. (b) RSoXS data at 285 eV from P3HT-*b*-PFTBT films cast from chloroform and annealed at 165 °C. A clear enhancement of scattering intensities along the plane of the polarization of the X-rays (horizontal axis) is evident. (c) RSoXS intensities versus scattering vector q for P3HT and P3HT-*b*-PFTBT. A broad peak near q^* ~ 0.03 Å^{-1} (21 nm) is apparent.

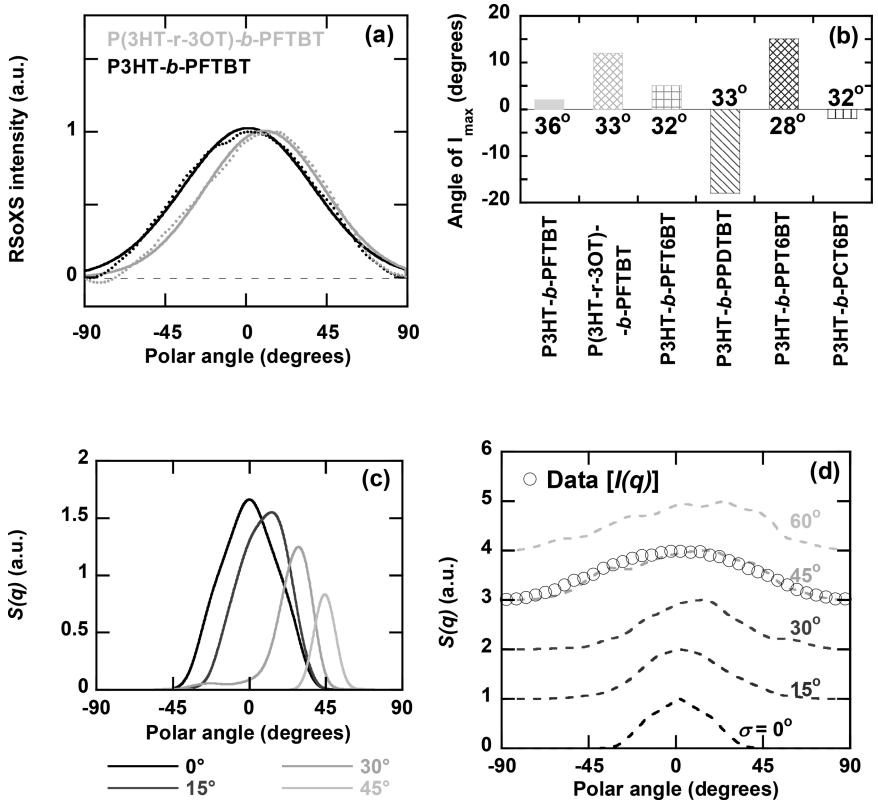

Figure 5. (a) RSoXS intensity at q = 0.031 1/Å as a function of polar angle for P3HT-*b*-PFTBT and P(3HT-r-3OT)-*b*-PFTBT. The maxima occur at about 2° and 15°, respectively. (b) Polar angle at maximum scattering intensity for each block copolymer used in this study, with the standard deviation σ shown above or below the bars. (c) Simulated RSoXS scattering plotted as a function of polar angle at the q^* peak for P3HT-*b*-PFTBT shown in Figure 3 with rotations of the P3HT blocks within lamella of 0°, 15°, 30°, and 45° from parallel to the P3HT/PFTBT interface. (d) Simulated RSoXS scattering plotted as a function of polar angle at the q^* peak for semicrystalline block copolymers shown in Figure 3, with rotation of the P3HT blocks within lamella of 2° from parallel to the P3HT/PFTBT interface and with varying degrees of dispersion in tilt. Simulations are shown with Gaussian dispersion in tilt with standard deviations ranging from of 0° to 60°. RSoXS data are also shown for P3HT-*b*-PFTBT (open circles).

although some contributions from mass and chemical contrast are expected.

Figure 4b shows RSoXS data for P3HT-*b*-PFTBT at 285 eV, where enhanced scattering in the direction parallel to the X-ray polarization is observed. Figure 4c shows the azimuthally averaged scattering profile for P3HT-*b*-PFTBT with a broad peak apparent at q = 0.03 Å^{-1}, corresponding to a domain spacing of ~20 nm. For comparison, scattering from P3HT is also shown in Figure 4c, where no features are apparent. Previous work has attributed the peak near q = 0.03 Å^{-1} to microphase separation in P3HT-*b*-PFTBT, without detailed analysis of the scattering anisotropy.[6,57,58]

Previous studies into the morphology of P3HT indicate backbone tilting within P3HT crystals.[24,59−61] Therefore, to properly access the true anisotropy of polymer systems, care must be taken to calculate the scattering at orthogonal angles that include the polar angle of maximum scattering intensity. We propose that the first step in calculating scattering anisotropy is to determine this angle of maximum intensity, corresponding to the backbone chain tilting of the polymer.

We can examine this angle that the chain backbones make with respect to domain interfaces by plotting the scattering intensity versus polar angle at a fixed q. The difference between the angle of maximum intensity when plotted against polar angle and 0° is the average tilt angle of the chain. Figure 5 compares the RSoXS intensity at q = 0.031 Å^{-1} for two block copolymers, P3HT-*b*-PFTBT and P(3HT-r-3OT)-*b*-PFTBT, where the peak in the intensity with polar angle differs. Figure 5b shows the angle at the maximum RSoXS intensity for the various block copolymers. As shown in Figure 5c, simulations of chains tilted within domains lead to peak intensities at polar angles that correspond to the tilt angle. Our simulations are in good agreement with the scattering data when we incorporate disorder in the tilt angle (Figure 5d). Thus, we attribute the angle for maximum intensity that ranges from −18° to 15° to correspond to the tilt angle of chains with respect to the block copolymer domain interface (Figure S8). This average backbone angle could correspond to a ring tilt within crystallites or an average backbone angle with respect to domain interfaces. Having found the maximum in scattering intensity with polar angle, we then calculate the scattering anisotropy obtained from our various polymers.

The RSoXS intensity of homopolymer P3HT also shows a peak away from zero polar angle (Figure S9). As P3HT has a negative anisotropy, the polar angle that corresponds to the minimum intensity is 12°, suggesting that, on average, rings within P3HT chains are tilted from the fibril short axis by 12°, a finding that has also been suggested from the crystal structure of P3HT.[60,62]

Scattering intensities centered at an angle away from 0° or 90° are observed for all six block copolymers (Figure S8) and in neat P3HT (Figure S9). Rotating or flipping the sample

does not affect the angle for scattering maxima (Figure S10), and changing the electric field polarization of the incident X-rays changes this scattering maxima angle accordingly. For a given polymer or block copolymer, the angle is also consistent across various experimental runs (Figure S11) and for samples that vary in the thickness of the polymer layer (Figure S12); thus, we conclude that the angular offsets of scattering intensities are not instrumental artifacts. As explored with our simulations, a possibility is that chains are tilted within domains, thereby leading to scattering intensity maxima at polar angles that correspond to the angle of the backbone (perpendicular to the TDM vector) with respect to domain interfaces.

A backbone tilt within crystals could arise from the density difference between semicrystalline and amorphous domains. To avoid large and unfavorable density disparities, chains can assemble at an angle with respect to the crystalline–amorphous interface.[63,64] These chain tilts have been shown to possess a correlation length of several semicrystalline chains, allowing for chain tilts to propagate from the interface due to high chain stiffness or crystallization nucleating at the interface.[65]

Previous work into the tilt angle of spin-coated semicrystalline block copolymer films has shown preferential orientation throughout the film.[66] This work suggests that the preferential tilt stems from constraints due to crystallization of one block within block copolymers. To alleviate packing stress, the crystalline backbones will tilt at domain boundaries, given the presence of semicrystalline–amorphous interfaces. Other work has suggested that polymer chains may be tilted through processing conditions such as surface effects that are a consequence of spin-coating.[67−72] Nevertheless, for our samples, the lack of dependence on the film thickness suggests that chain tilt occurs within the bulk of the film.

If backbones are angled with respect to domain interfaces, we expect that chains would be equally likely to exhibit positive and negative tilts. In Figure S13, we include an equal probability of positive and negative chain angles in our scattering simulations. Two peaks in the data corresponding to positive and negative polar angles are apparent. In contrast, our experimental results always show a single scattering maximum with respect to the polar angle. This breaking of symmetry could be explained by a mesoscale chirality. We speculate that tie chains between crystalline regions and across domains establish a small degree of correlation in chain tilt between adjacent domains; in block copolymers, this would imply a triblock copolymer impurity that connects two crystalline regions.[40] Indeed, RSoXS intensities are broad with respect to polar angle, suggesting a broad distribution of tilt angles, including positive and negative angles.

As mentioned earlier, the invariance of scattering with sample rotation demonstrates a lack of global alignment, such that RSoXS anisotropy is due to the local structure. Furthermore, the invariance with flipping the sample from front to back (Figure S10) also suggests the sign of the tilt angle does not depend on the sample geometry. We hypothesize that a helical structure such as from a cholesteric phase, as has been previously demonstrated for other semicrystalline-amorphous polymers, could explain our scattering results.[73−76] The helical mesoscale structure would produce an anisotropic scattering pattern, with a scattering intensity maximum at a positive or negative angle if only right-handed or left-handed helices are present, as has been previously shown.[76] The presence of multiple local helical structures, in our case potentially loosely connected by tie chains, would produce a scattering maximum at either a positive or negative polar angle, regardless of the orientation of the substrate. These connected helical structures can be stretched upon heating or annealing, leading to a preferential texturing within the mesoscale and "barber pole" structures.[77] A schematic of this potential morphology is shown in Figure S14. Further work is needed to explore whether such a structure is present in our block copolymer thin films.

Having established the polar angle for maximum RSoXS intensity, we calculate the scattering anisotropy of P3HT and P3HT-*b*-PFTBT. We use scattering intensities that are parallel or perpendicular with respect to the angle of max intensity:

$$A_{\text{expt}}(q) = \frac{I_{\theta+0^\circ}(q) - I_{\theta+90^\circ}(q)}{I_{\theta+0^\circ}(q) + I_{\theta+90^\circ}(q)} \quad (3)$$

where $A_{\text{expt}}(q)$ is the anisotropy ratio as a function of q and $I_i(q)$ is the scattering intensity at a specific polar angle; in this case, 0° for $I_{\theta+0^\circ}(q)$ and 90° for $I_{\theta+90^\circ}(q)$ were used. Figure 6 shows $A_{\text{expt}}(q)$ for P3HT homopolymer and P3HT-*b*-PFTBT (further details on calculating $A_{\text{expt}}(q)$ can be found in Figures S15–S17). P3HT anisotropy shows a negative peak at approximately q = 0.03 Å^{-1}, which we compare to our model for semicrystalline P3HT shown in Figure 2; the negative anisotropy suggests molecular orbitals parallel and backbones perpendicular to the crystalline/amorphous interface. Chains perpendicular to the crystal surface are consistent with the predominant structural models of P3HT fibril-like crystals.[78−80] Thus, we attribute this peak to the crystal spacing that is sometimes apparent in the scattering from semicrystalline polymers.[81,82]

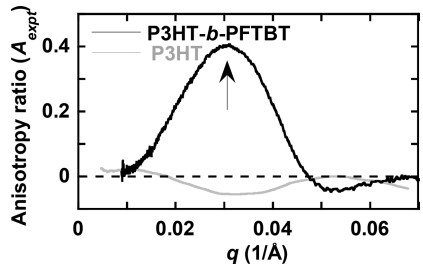

Figure 6. Anisotropy ratio calculated from RSoXS scattering at 285 eV versus q for P3HT-*b*-PFTBT (black) and P3HT (gray) films cast from chloroform. Both data show a peak near q = 0.03 Å^{-1}, although the anisotropy is negative for P3HT and positive for P3HT-*b*-PFTBT. The peak in the anisotropy is at the same q as the scattering peak shown in Figure 3. A negative peak is also seen in the anisotropy ratio for P3HT-*b*-PFTBT near 0.058 Å^{-1}.

In contrast, P3HT-*b*-PFTBT anisotropy is positive near q = 0.03 Å^{-1}, but also shows a small negative peak at q = 0.06 Å^{-1}. Comparing to our model for P3HT-*b*-PFTBT shown in Figure 3, we attribute the positive anisotropy to domains with chains parallel to domain interfaces and the negative anisotropy to chains perpendicular to the interface; chains are expected to align parallel to interfaces of semiflexible polymers.[83,84] The peak in the anisotropy near q = 0.03 Å^{-1} corresponds to the feature in $I(q)$ shown in Figure 4c, suggesting that this peak corresponds to the domain spacing of a block copolymer mesophase. The negative anisotropy near q = 0.06 Å^{-1} could correspond to the spacing between crystals within P3HT

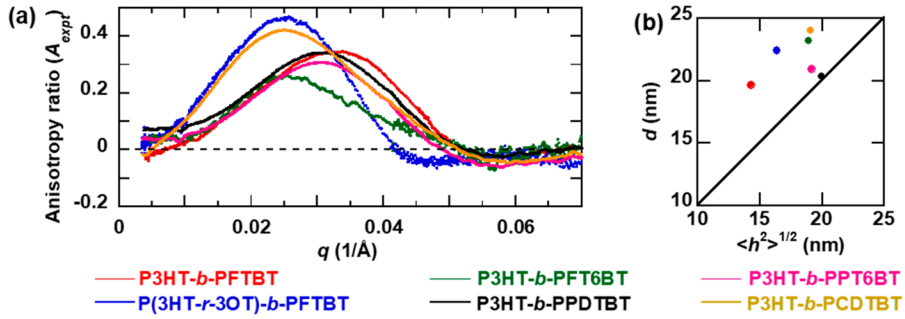

Figure 7. (a) Anisotropy ratio versus scattering vector q for various block copolymers at an X-ray energy of 285 eV. (b) d spacing extracted from peak in anisotropy data versus estimated end-to-end distance of block copolymer chains.

domains, similarly to what we observe in P3HT homopolymers but with a smaller spacing between crystals; the slight negative anisotropy at this q is confirmed by examining scattering as a function of polar angle, as shown in Figure S18.

The scattering anisotropy for the block copolymers in Figure 1 is shown in Figure 7. Data were taken at 285 eV, which leads to the maximum contrast in all block copolymers due to the similarity between the donor blocks (Figure S7). All six block copolymers exhibit a positive peak between q = 0.02 Å^{-1} and q = 0.03 Å^{-1} and nearly all show a smaller, negative peak around q = 0.06 Å^{-1}, suggesting a similar structure. We extract the domain spacing from the positive peak in the anisotropy and compare this spacing to estimated values for the end-to-end distance ($\langle h^2 \rangle^{1/2}$) of the block copolymers. Average end-to-end distances were calculated using molecular weights from nuclear magnetic resonance (NMR) and gel permeation chromatography (GPC) (Table S1) and persistence lengths from simulations.[85,86] As shown in Figure 7b, there is good agreement between the domain spacing and the average end-to-end spacing.

For flexible block copolymers with lamellar morphologies, chains assemble themselves end-to-end, such that the domain spacing roughly scales with twice the end-to-end distance of the chains.[81] Thus, Figure 7b suggests that chains intercalate within lamellar block copolymer domains, which could be a consequence of the thin cross section of conjugated polymers compared to flexible chains. The agreement with the end-to-end distance calculated with an exponent of 1/2 would then suggest weak microphase separation, which has been speculated in similar block copolymers.[87−89] Alternatively, the correspondence of the end-to-end distance with the domain spacing could also suggest a cylindrical morphology, although lamellar phases are expected to dominate the phase behavior of semiflexible block copolymers.[90] Nevertheless, the correlation between the end-to-end distance and the domain spacing from RSoXS supports our assignment of the peak in anisotropy between q = 0.02 Å^{-1} and q = 0.03 Å^{-1} to the microphase separation in block copolymers.

On the basis of our analysis of the scattering anisotropy and scattering intensity with polar angle, we summarize the average chain alignment within P3HT and P3HT block copolymer domains in Figure 8. Figures 8a and 8b are shown as top-down views of the polymer films, showing the semicrystalline P3HT chains as blue lines and the P3HT and PFTBT domains as blue and red regions, respectively. We envision P3HT backbones as roughly perpendicular to interfaces and tilted by 12° within fibrils, and because we only observe a single scattering maxima with polar angle, this tilt is correlated between adjacent domains. As previously discussed, this local

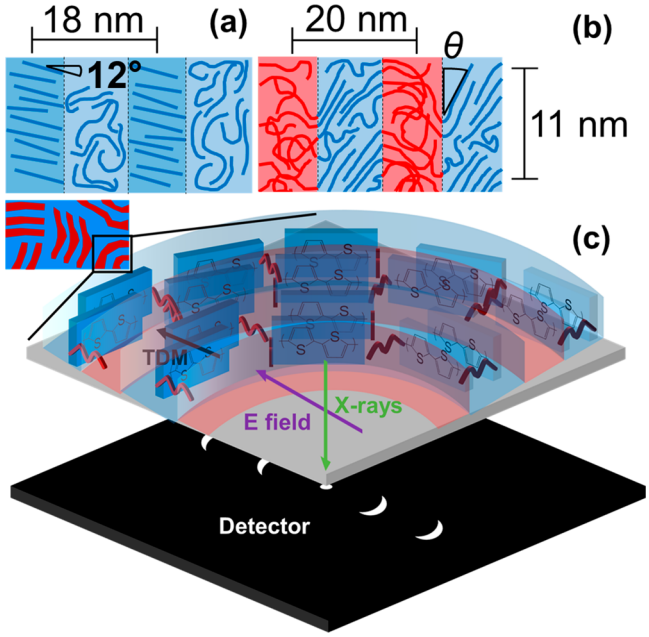

Figure 8. (a) Depiction of neat P3HT microstructure determined from RSoXS from a top-down view. Blue regions are amorphous P3HT, and P3HT crystals are also shown as blue lines. From Figures 2 and 5, the negative anisotropy near $q \sim 0.034$ Å^{-1} suggests an 18 nm spacing of P3HT crystals. In (b), a depiction of P3HT-*b*-PFTBT microstructure determined from RSoXS is shown, also from a top-down view. Blue regions again represent amorphous P3HT with semicrystalline regions of P3HT shown as blue lines and the amorphous PFTBT shown in red. From Figures 3 and 5, the positive anisotropy near $q \sim 0.032$ Å^{-1} suggests a 20 nm spacing of microphase-separated domains and the negative anisotropy near $q \sim 0.06$ Å^{-1} suggests an 11 nm spacing between crystals in P3HT domains. The angle θ represents the degree of offset of the P3HT rings with respect to the interface. In conjugated block copolymers such as P3HT-*b*-PFTBT, a chain or ring tilt of 2° to 20° is apparent. (c) Schematic of block copolymer domains highlighting the geometrical relationship between the TDM of P3HT and the propagation and polarization direction of incident X-rays. Microphase-separated domains oriented with the TDM parallel to the X-ray polarization will exhibit enhanced scattering, as shown in the inset, with the X-rays (green arrow) transmitting through the sample and the E field being in the plane of the sample, perpendicular to the opaque chain backbones.

correlation of chain tilts could be due to stiff backbones and tie chains between crystallites. In our block copolymers, whose cross section is shown Figure 8b, we also observe chain tilts within the semicrystalline domains, but with backbones nearly

parallel to block copolymer domain interfaces. We speculate this is a balance of the tendency for semiflexible chains to align parallel near interfaces[91] and the need for the block copolymer junction to be localized for mesoscale self-assembly. The contour lengths of our P3HT chains range from 12 to 17 nm, such that the broad distribution in backbone angles (Figure 5d) and the stiff backbones allows for space filling of ∼10 nm domains, even when chains are on average parallel to the interface. Our block copolymers exhibit significant dispersity and compositional dispersity, which may aid in packing.[40] The single scattering maxima with polar angle suggest local correlations between backbone tilts, but the invariance with flipping the sample from front to back suggests a complex structure (Figure S10). Although further work is needed to reveal the higher-order assembly in these block copolymers, we propose one possible explanation is that of a mesoscale helical structure (Figure S14).

CONCLUSIONS

RSoXS is a powerful tool to characterize the microstructure in thin films of soft materials because of the potential to increase the contrast based on differences in density, chemical composition, bonding, and chain orientation. The analysis presented here demonstrates an approach to determine domain spacings from peaks in the scattering anisotropy, chain orientation within domains from the sign of the anisotropy, and average chain tilt from maxima or minima in scattering intensities with polar angle. With a combination of scattering simulations and experiments, we demonstrate that RSoXS contrast can be due to differences in chemical composition or average orientation of chains within domains. We thus predict that profiles from linearly polarized RSoXS at resonance with locally aligned TDMs are equivalent to scattering patterns from aligned microstructures. For P3HT-*b*-PFTBT and similar block copolymers, we find a roughly 20 nm domain spacing due to microphase separation and a roughly 10 nm spacing between crystals within P3HT. We show that within block copolymer mesophases chains are aligned nearly parallel to domain interfaces; this has been predicted from theory and simulations but has not been experimentally shown previously. P3HT homopolymer chains are perpendicular to the fibril axis, with rings that are tilted by about 12°, which is consistent to our current understanding of the crystal structure of P3HT.

ASSOCIATED CONTENT

Supporting Information

The Supporting Information is available free of charge on the ACS Publications website at DOI: 10.1021/acs.macromol.8b02198.

Simulations of P3HT at perpendicular scattering vectors; methods for suppressing anisotropy or molecular ordering; chemical contrast of P3HT-*b*-PFTBT; fitted scattering intensities as a function of polar angle to identify isotropic line; molecular weights and persistence lengths of block copolymers; chain tilt of polymers; GIWAXS of homopolymers and block copolymers (PDF)

AUTHOR INFORMATION

Corresponding Author

*E-mail edg12@psu.edu.

ORCID

Qing Wang: 0000-0002-5968-3235

Enrique D. Gomez: 0000-0001-8942-4480

Notes

The authors declare no competing financial interest.

ACKNOWLEDGMENTS

Financial support from the National Science Foundation under Award DMR-1626566 is acknowledged. Financial support from the Office of Naval Research under Grant N000141410532 is also acknowledged. The Advanced Light Source is supported by the Director, Office of Science, Office of Basic Energy Sciences, of the U.S. Department of Energy under Contract DE-AC02-05CH11231. B.K. acknowledges support from the ALS Doctoral Fellowship in Residence.

REFERENCES

(1) Brédas, J.-L.; Norton, J. E.; Cornil, J.; Coropceanu, V. Molecular understanding of organic solar cells: the challenges. *Acc. Chem. Res.* **2009**, *42* (11), 1691−1699.

(2) Forrest, S. R. The path to ubiquitous and low-cost organic electronic appliances on plastic. *Nature* **2004**, *428* (6986), 911.

(3) Günes, S.; Neugebauer, H.; Sariciftci, N. S. Conjugated polymer-based organic solar cells. *Chem. Rev.* **2007**, *107* (4), 1324−1338.

(4) Mayer, A. C.; Scully, S. R.; Hardin, B. E.; Rowell, M. W.; McGehee, M. D. Polymer-based solar cells. *Mater. Today* **2007**, *10* (11), 28−33.

(5) Scharber, M. C.; Mühlbacher, D.; Koppe, M.; Denk, P.; Waldauf, C.; Heeger, A. J.; Brabec, C. J. Design rules for donors in bulk-heterojunction solar cells—Towards 10% energy-conversion efficiency. *Adv. Mater.* **2006**, *18* (6), 789−794.

(6) Guo, C.; Lin, Y.-H.; Witman, M. D.; Smith, K. A.; Wang, C.; Hexemer, A.; Strzalka, J.; Gomez, E. D.; Verduzco, R. Conjugated block copolymer photovoltaics with near 3% efficiency through microphase separation. *Nano Lett.* **2013**, *13* (6), 2957−2963.

(7) Korevaar, P. A.; Grenier, C.; Markvoort, A. J.; Schenning, A. P.; de Greef, T. F.; Meijer, E. Model-driven optimization of multi-component self-assembly processes. *Proc. Natl. Acad. Sci. U. S. A.* **2013**, *110* (43), 17205−17210.

(8) Kaur, N.; Singh, M.; Pathak, D.; Wagner, T.; Nunzi, J. Organic materials for photovoltaic applications: Review and mechanism. *Synth. Met.* **2014**, *190*, 20−26.

(9) Gehan, T. S.; Bag, M.; Renna, L. A.; Shen, X.; Algaier, D. D.; Lahti, P. M.; Russell, T. P.; Venkataraman, D. Multiscale active layer morphologies for organic photovoltaics through self-assembly of nanospheres. *Nano Lett.* **2014**, *14* (9), 5238−5243.

(10) Engmann, S.; Machalett, M.; Turkovic, V.; Rösch, R.; Rädlein, E.; Gobsch, G.; Hoppe, H. Photon recycling across a ultraviolet-blocking layer by luminescence in polymer solar cells. *J. Appl. Phys.* **2012**, *112* (3), 034517.

(11) Engmann, S.; Singh, C. R.; Turkovic, V.; Hoppe, H.; Gobsch, G. Direct Correlation of the Organic Solar Cell Device Performance to the In-Depth Distribution of Highly Ordered Polymer Domains in Polymer/Fullerene Films. *Adv. Energy Mater.* **2013**, *3* (11), 1463−1472.

(12) Collins, B. A.; Gann, E.; Guignard, L.; He, X.; McNeill, C. R.; Ade, H. Molecular miscibility of polymer− fullerene blends. *J. Phys. Chem. Lett.* **2010**, *1* (21), 3160−3166.

(13) Darling, S. B. Block copolymers for photovoltaics. *Energy Environ. Sci.* **2009**, *2* (12), 1266−1273.

(14) Bates, F. S.; Fredrickson, G. H. Block copolymers-designer soft materials. *Phys. Today* **1999**, *52*, 32.

(15) Topham, P. D.; Parnell, A. J.; Hiorns, R. C. Block copolymer strategies for solar cell technology. *J. Polym. Sci., Part B: Polym. Phys.* **2011**, *49* (16), 1131−1156.

(16) Tseng, Y.-C.; Darling, S. B. Block copolymer nanostructures for technology. *Polymers* **2010**, *2* (4), 470−489.

(17) Sun, S.; Fan, Z.; Wang, Y.; Haliburton, J.; Taft, C.; Maaref, S.; Seo, K.; Bonner, C. Conjugated block copolymers for opto-electronic functions. *Synth. Met.* **2003**, *137* (1−3), 883−884.
(18) Sommer, M.; Huettner, S.; Thelakkat, M. Donor−acceptor block copolymers for photovoltaic applications. *J. Mater. Chem.* **2010**, *20* (48), 10788−10797.
(19) Vakhshouri, K.; Smith, B. H.; Chan, E. P.; Wang, C.; Salleo, A.; Wang, C.; Hexemer, A.; Gomez, E. D. Signatures of Intracrystallite and Intercrystallite Limitations of Charge Transport in Polythiophenes. *Macromolecules* **2016**, *49* (19), 7359−7369.
(20) Vakhshouri, K.; Kesava, S. V.; Kozub, D. R.; Gomez, E. D. Characterization of the mesoscopic structure in the photoactive layer of organic solar cells: A focused review. *Mater. Lett.* **2013**, *90*, 97−102.
(21) DeLongchamp, D. M.; Kline, R. J.; Fischer, D. A.; Richter, L. J.; Toney, M. F. Molecular characterization of organic electronic films. *Adv. Mater.* **2011**, *23* (3), 319−337.
(22) Potemkin, I. I.; Busch, P.; Smilgies, D. M.; Posselt, D.; Papadakis, C. M. Effect of the molecular weight of AB diblock copolymers on the lamellar orientation in thin films: Theory and experiment. *Macromol. Rapid Commun.* **2007**, *28* (5), 579−584.
(23) Gevaerts, V. S.; Herzig, E. M.; Kirkus, M.; Hendriks, K. H.; Wienk, M. M.; Perlich, J.; Müller-Buschbaum, P.; Janssen, R. A. Influence of the position of the side chain on crystallization and solar cell performance of DPP-based small molecules. *Chem. Mater.* **2014**, *26* (2), 916−926.
(24) Salleo, A.; Kline, R. J.; DeLongchamp, D. M.; Chabinyc, M. L. Microstructural characterization and charge transport in thin films of conjugated polymers. *Adv. Mater.* **2010**, *22* (34), 3812−3838.
(25) Quiram, D. J.; Register, R. A.; Marchand, G. R.; Adamson, D. H. Chain orientation in block copolymers exhibiting cylindrically confined crystallization. *Macromolecules* **1998**, *31* (15), 4891−4898.
(26) Rangarajan, P.; Register, R. A.; Adamson, D. H.; Fetters, L. J.; Bras, W.; Naylor, S.; Ryan, A. J. Dynamics of structure formation in crystallizable block copolymers. *Macromolecules* **1995**, *28* (5), 1422−1428.
(27) Rangarajan, P.; Register, R. A.; Fetters, L. J. Morphology of semicrystalline block copolymers of ethylene-(ethylene-alt-propylene). *Macromolecules* **1993**, *26* (17), 4640−4645.
(28) Ryan, A. J.; Fairclough, J. P. A.; Hamley, I. W.; Mai, S.-M.; Booth, C. Chain folding in crystallizable block copolymers. *Macromolecules* **1997**, *30* (6), 1723−1727.
(29) Swaraj, S.; Wang, C.; Araki, T.; Mitchell, G.; Liu, L.; Gaynor, S.; Deshmukh, B.; Yan, H.; McNeill, C.; Ade, H. The utility of resonant soft x-ray scattering and reflectivity for the nanoscale characterization of polymers. *Eur. Phys. J.: Spec. Top.* **2009**, *167* (1), 121−126.
(30) Gann, E.; Young, A.; Collins, B.; Yan, H.; Nasiatka, J.; Padmore, H.; Ade, H.; Hexemer, A.; Wang, C. Soft x-ray scattering facility at the Advanced Light Source with real-time data processing and analysis. *Rev. Sci. Instrum.* **2012**, *83* (4), 045110.
(31) Virgili, J.; Kortright, J.; Balsara, N.; Segalman, R. In Structural Characterization of Asymmetric Block Copolymer Thin Films using Resonant Soft X-Ray Scattering, APS Meeting Abstracts, 2007; 2007.
(32) Virgili, J. M.; Tao, Y.; Kortright, J. B.; Balsara, N. P.; Segalman, R. A. Analysis of order formation in block copolymer thin films using resonant soft X-ray scattering. *Macromolecules* **2007**, *40* (6), 2092−2099.
(33) Guo, C.; Kozub, D. R.; Vajjala Kesava, S.; Wang, C.; Hexemer, A.; Gomez, E. D. Signatures of multiphase formation in the active layer of organic solar cells from resonant soft x-ray scattering. *ACS Macro Lett.* **2013**, *2* (3), 185−189.
(34) Wang, C.; Lee, D. H.; Hexemer, A.; Kim, M. I.; Zhao, W.; Hasegawa, H.; Ade, H.; Russell, T. P. Defining the Nanostructured Morphology of Triblock Copolymers Using Resonant Soft X-ray Scattering. *Nano Lett.* **2011**, *11* (9), 3906−3911.
(35) Swaraj, S.; Wang, C.; Yan, H.; Watts, B.; Luning, J.; McNeill, C. R.; Ade, H. Nanomorphology of bulk heterojunction photovoltaic thin films probed with resonant soft X-ray scattering. *Nano Lett.* **2010**, *10* (8), 2863−2869.
(36) Collins, B.; Cochran, J.; Yan, H.; Gann, E.; Hub, C.; Fink, R.; Wang, C.; Schuettfort, T.; McNeill, C.; Chabinyc, M.; Ade, H. Polarized X-ray scattering reveals non-crystalline orientational ordering in organic films. *Nat. Mater.* **2012**, *11* (6), 536.
(37) Gann, E.; Collins, B. A.; Tang, M.; Tumbleston, J. R.; Mukherjee, S.; Ade, H. Origins of polarization-dependent anisotropic X-ray scattering from organic thin films. *J. Synchrotron Radiat.* **2016**, *23* (1), 219−227.
(38) Stone, K. H.; Kortright, J. B. Molecular anisotropy effects in carbon K-edge scattering: Depolarized diffuse scattering and optical anisotropy. *Phys. Rev. B: Condens. Matter Mater. Phys.* **2014**, *90* (10), 104201.
(39) Lin, Y.-H.; Smith, K. A.; Kempf, C. N.; Verduzco, R. Synthesis and crystallinity of all-conjugated poly (3-hexylthiophene) block copolymers. *Polym. Chem.* **2013**, *4* (2), 229−232.
(40) Lee, Y.; Aplan, M.; Kilbey, S. M. M.; Seibers, Z.; Wang, Q.; Gomez, E. D. Tuning the synthesis of fully conjugated block copolymers to minimize architectural heterogeneity. *J. Mater. Chem. A* **2017**, *5* (38), 20412−20421.
(41) Aplan, M. P.; Munro, J. M.; Lee, Y.; Brigeman, A. N.; Grieco, C.; Wang, Q.; Giebink, N. C.; Dabo, I.; Asbury, J. B.; Gomez, E. D. Revealing the Importance of Energetic and Entropic Contributions to the Driving Force for Charge Photogeneration. *ACS Appl. Mater. Interfaces* **2018**, *10* (46), 39933−39941.
(42) Hu, Z.; Gesquiere, A. J. PCBM concentration dependent morphology of P3HT in composite P3HT/PCBM nanoparticles. *Chem. Phys. Lett.* **2009**, *476* (1), 51−55.
(43) Biniek, L.; Schwartz, P.-O.; Zaborova, E.; Heinrich, B.; Leclerc, N.; Méry, S.; Brinkmann, M. Zipper-like molecular packing of donor−acceptor conjugated co-oligomers based on perylenediimide. *J. Mater. Chem. C* **2015**, *3* (14), 3342−3349.
(44) Feng, J.; Yan, X.; Liu, Y.; Gao, H.; Wu, Y.; Su, B.; Jiang, L. Crystallographically Aligned Perovskite Structures for High-Performance Polarization-Sensitive Photodetectors. *Adv. Mater.* **2017**, *29* (16), 1605993.
(45) Yoon, E.; Gong, J.; Jung, Y.; Lee, W.; Driver, R. W.; Lee, H.-S. Unambiguous characterization of anisotropic foldamer packing in a foldecture with an elongated hexagonal plate shape. *Chem. Commun.* **2016**, *52* (30), 5250−5253.
(46) Zhao, Y.; Fan, X.; Feng, J.; Wang, X.; Wu, Y.; Su, B.; Jiang, L. Regulated Dewetting for Patterning Organic Single Crystals with Pure Crystallographic Orientation toward High Performance Field-Effect Transistors. *Adv. Funct. Mater.* **2018**, *28*, 1800470.
(47) Kaiser, G. *A Friendly Guide to Wavelets*; Springer Science & Business Media: 2010.
(48) Rahman, M. *Applications of Fourier Transforms to Generalized Functions*; WIT Press: 2011.
(49) Yarnell, J.; Katz, M.; Wenzel, R. G.; Koenig, S. Structure factor and radial distribution function for liquid argon at 85 K. *Phys. Rev. A: At., Mol., Opt. Phys.* **1973**, *7* (6), 2130.
(50) Tumbleston, J. R.; Collins, B. A.; Yang, L.; Stuart, A. C.; Gann, E.; Ma, W.; You, W.; Ade, H. The influence of molecular orientation on organic bulk heterojunction solar cells. *Nat. Photonics* **2014**, *8* (5), 385.
(51) Carpenter, J. H.; Hunt, A.; Ade, H. Characterizing morphology in organic systems with resonant soft X-ray scattering. *J. Electron Spectrosc. Relat. Phenom.* **2015**, *200*, 2−14.
(52) Van Dommelen, J.; Brekelmans, W.; Baaijens, F. Micromechanical modeling of particle-toughening of polymers by locally induced anisotropy. *Mech. Mater.* **2003**, *35* (9), 845−863.
(53) Ma, W.; Reinspach, J.; Zhou, Y.; Diao, Y.; McAfee, T.; Mannsfeld, S. C.; Bao, Z.; Ade, H. Tuning local molecular orientation−composition correlations in binary organic thin films by solution shearing. *Adv. Funct. Mater.* **2015**, *25* (21), 3131−3137.
(54) Mane, J. M.; Le Normand, F.; Medjo, R. E.; Cojocaru, C. S.; Ersen, O.; Senger, A.; Laffon, C.; Sendja, B. T.; Biouele, C. M.; Ben-Bolie, G. H.; Ateba, P. O.; Parent, P. Alignment of vertically grown carbon nanostructures studied by X-ray absorption spectroscopy. *Mater. Sci. Appl.* **2014**, *5* (13), 966.

(55) Sendja, B. T.; Medjo, R. E.; Mane, J. M.; Ben-Bolie, G. H.; Ateba, P. O. Theoretical Investigation of X-Ray Absorption near Edge Spectroscopy (XANES) Angular Dependence of Aligned Carbon Nanotubes Grown by DC HF CVD Process. *Mater. Sci. Appl.* **2015**, *6* (05), 373.
(56) Ade, H. Characterization of organic thin films with resonant soft X-ray scattering and reflectivity near the carbon and fluorine absorption edges. *Eur. Phys. J.: Spec. Top.* **2012**, *208* (1), 305−318.
(57) Guo, C.; Lee, Y.; Lin, Y.-H.; Strzalka, J.; Wang, C.; Hexemer, A.; Jaye, C.; Fischer, D. A.; Verduzco, R.; Wang, Q.; Gomez, E. D. Photovoltaic Performance of Block Copolymer Devices Is Independent of the Crystalline Texture in the Active Layer. *Macromolecules* **2016**, *49* (12), 4599−4608.
(58) Grieco, C.; Aplan, M. P.; Rimshaw, A.; Lee, Y.; Le, T. P.; Zhang, W.; Wang, Q.; Milner, S. T.; Gomez, E. D.; Asbury, J. B. Molecular Rectification in Conjugated Block Copolymer Photovoltaics. *J. Phys. Chem. C* **2016**, *120* (13), 6978−6988.
(59) Himmelberger, S.; Duong, D. T.; Northrup, J. E.; Rivnay, J.; Koch, F. P.; Beckingham, B. S.; Stingelin, N.; Segalman, R. A.; Mannsfeld, S. C.; Salleo, A. Role of Side-Chain Branching on Thin-Film Structure and Electronic Properties of Polythiophenes. *Adv. Funct. Mater.* **2015**, *25* (17), 2616−2624.
(60) Kayunkid, N.; Uttiya, S.; Brinkmann, M. Structural model of regioregular poly (3-hexylthiophene) obtained by electron diffraction analysis. *Macromolecules* **2010**, *43* (11), 4961−4967.
(61) Maillard, A.; Rochefort, A. Structural and electronic properties of poly (3-hexylthiophene) π-stacked crystals. *Phys. Rev. B: Condens. Matter Mater. Phys.* **2009**, *79* (11), 115207.
(62) Dudenko, D.; Kiersnowski, A.; Shu, J.; Pisula, W.; Sebastiani, D.; Spiess, H. W.; Hansen, M. R. A Strategy for Revealing the Packing in Semicrystalline Π-Conjugated Polymers: Crystal Structure of Bulk Poly-3-Hexyl-Thiophene (P3HT). *Angew. Chem., Int. Ed.* **2012**, *51* (44), 11068−11072.
(63) Fritzsching, K. J.; Mao, K.; Schmidt-Rohr, K. Avoidance of density anomalies as a structural principle for semicrystalline polymers: the importance of chain ends and chain tilt. *Macromolecules* **2017**, *50* (4), 1521−1540.
(64) Remy, R.; Wei, S.; Campos, L. M.; Mackay, M. E. Three-Phase Morphology of Semicrystalline Polymer Semiconductors: A Quantitative Analysis. *ACS Macro Lett.* **2015**, *4* (9), 1051−1055.
(65) Hammond, M. R.; Kline, R. J.; Herzing, A. A.; Richter, L. J.; Germack, D. S.; Ro, H.-W.; Soles, C. L.; Fischer, D. A.; Xu, T.; Yu, L.; Toney, M. F.; DeLongchamp, D. M. Molecular order in high-efficiency polymer/fullerene bulk heterojunction solar cells. *ACS Nano* **2011**, *5* (10), 8248−8257.
(66) Busch, P.; Krishnan, S.; Paik, M.; Toombes, G. E.; Smilgies, D.-M.; Gruner, S. M.; Ober, C. K. Surface induced tilt propagation in thin films of semifluorinated liquid crystalline side chain block copolymers. *Macromolecules* **2007**, *40* (1), 81−89.
(67) Tanaka, K.; Takahara, A.; Kajiyama, T. Film thickness dependence of the surface structure of immiscible polystyrene/poly (methyl methacrylate) blends. *Macromolecules* **1996**, *29* (9), 3232−3239.
(68) Sundrani, D.; Darling, S.; Sibener, S. Guiding polymers to perfection: macroscopic alignment of nanoscale domains. *Nano Lett.* **2004**, *4* (2), 273−276.
(69) Seo, D.-S.; Araya, K.; Yoshida, N.; Nishikawa, M.; Yabe, Y.; Kobayashi, S. Effect of the polymer tilt angle for generation of pretilt angle in nematic liquid crystal on rubbed polyimide surfaces. *Jpn. J. Appl. Phys.* **1995**, *34* (4B), L503.
(70) Kline, R. J.; McGehee, M. D.; Toney, M. F. Highly oriented crystals at the buried interface in polythiophene thin-film transistors. *Nat. Mater.* **2006**, *5* (3), 222.
(71) Geary, J.; Goodby, J.; Kmetz, A.; Patel, J. The mechanism of polymer alignment of liquid-crystal materials. *J. Appl. Phys.* **1987**, *62* (10), 4100−4108.
(72) Schuettfort, T.; Thomsen, L.; McNeill, C. R. Observation of a distinct surface molecular orientation in films of a high mobility conjugated polymer. *J. Am. Chem. Soc.* **2013**, *135* (3), 1092−1101.
(73) Chen, D.; Porada, J. H.; Hooper, J. B.; Klittnick, A.; Shen, Y.; Tuchband, M. R.; Korblova, E.; Bedrov, D.; Walba, D. M.; Glaser, M. A.; Maclennan, J. E.; Clark, N. A. Chiral heliconical ground state of nanoscale pitch in a nematic liquid crystal of achiral molecular dimers. *Proc. Natl. Acad. Sci. U. S. A.* **2013**, *110*, 15931.
(74) Zhu, C.; Wang, C.; Young, A.; Liu, F.; Gunkel, I.; Chen, D.; Walba, D.; Maclennan, J.; Clark, N.; Hexemer, A. Probing and controlling liquid crystal helical nanofilaments. *Nano Lett.* **2015**, *15* (5), 3420−3424.
(75) Zhu, C.; Tuchband, M. R.; Young, A.; Shuai, M.; Scarbrough, A.; Walba, D. M.; Maclennan, J. E.; Wang, C.; Hexemer, A.; Clark, N. A. Resonant carbon K-edge soft X-ray scattering from lattice-free heliconical molecular ordering: soft dilative elasticity of the twist-bend liquid crystal phase. *Phys. Rev. Lett.* **2016**, *116* (14), 147803.
(76) Salamończyk, M.; Vaupotič, N.; Pociecha, D.; Wang, C.; Zhu, C.; Gorecka, E. Structure of nanoscale-pitch helical phases: blue phase and twist-bend nematic phase resolved by resonant soft X-ray scattering. *Soft Matter* **2017**, *13* (38), 6694−6699.
(77) Tuchband, M. R.; Shuai, M.; Graber, K. A.; Chen, D.; Zhu, C.; Radzihovsky, L.; Klittnick, A.; Foley, L. M.; Scarbrough, A.; Porada, J. H. Double-Helical Tiled Chain Structure of the Twist-Bend Liquid Crystal phase in CB7CB. arXiv preprint arXiv:1703.10787, 2017.
(78) Vakhshouri, K.; Smith, B. H.; Chan, E. P.; Wang, C. C.; Salleo, A.; Wang, C.; Hexemer, A.; Gomez, E. D. Signatures of Intracrystallite and Intercrystallite Limitations of Charge Transport in Polythiophenes. *Macromolecules* **2016**, *49* (19), 7359−7369.
(79) Yang, H.; Shin, T. J.; Yang, L.; Cho, K.; Ryu, C. Y.; Bao, Z. Effect of Mesoscale Crystalline Structure on the Field-Effect Mobility of Regioregular Poly(3-hexyl thiophene) in Thin-Film Transistors. *Adv. Funct. Mater.* **2005**, *15* (4), 671−676.
(80) Prosa, T. J.; Winokur, M. J.; Moulton, J.; Smith, P.; Heeger, A. J. X-Ray structural studies of poly(3-alkylthiophenes) - an example of an inverse comb. *Macromolecules* **1992**, *25* (17), 4364−4372.
(81) Strobl, G. *The Physics of Polymers*; Springer: Berlin, 2007.
(82) Zhang, R.; Li, B.; Iovu, M. C.; Jeffries-El, M.; Sauve, G.; Cooper, J.; Jia, S. J.; Tristram-Nagle, S.; Smilgies, D. M.; Lambeth, D. N.; McCullough, R. D.; Kowalewski, T. Nanostructure dependence of field-effect mobility in regioregular poly(3-hexylthiophene) thin film field effect transistors. *J. Am. Chem. Soc.* **2006**, *128* (11), 3480−3481.
(83) Zhang, W. L.; Gomez, E. D.; Milner, S. T. Surface-Induced Chain Alignment of Semiflexible Polymers. *Macromolecules* **2016**, *49* (3), 963−971.
(84) Morse, D. C.; Fredrickson, G. H. Semiflexible polymers near interfaces. *Phys. Rev. Lett.* **1994**, *73* (24), 3235−3238.
(85) Kuei, B.; Gomez, E. D. Chain conformations and phase behavior of conjugated polymers. *Soft Matter* **2017**, *13* (1), 49−67.
(86) Zhang, W.; Gomez, E. D.; Milner, S. T. Predicting Chain Dimensions of Semiflexible Polymers from Dihedral Potentials. *Macromolecules* **2014**, *47* (18), 6453−6461.
(87) Leibler, L. Theory of microphase separation in block copolymers. *Macromolecules* **1980**, *13* (6), 1602−1617.
(88) Lombeck, F.; Komber, H.; Sepe, A.; Friend, R. H.; Sommer, M. Enhancing Phase Separation and Photovoltaic Performance of All-Conjugated Donor−Acceptor Block Copolymers with Semifluorinated Alkyl Side Chains. *Macromolecules* **2015**, *48* (21), 7851−7860.
(89) Sommer, M.; Komber, H.; Huettner, S.; Mulherin, R.; Kohn, P.; Greenham, N. C.; Huck, W. T. Synthesis, purification, and characterization of well-defined all-conjugated diblock copolymers PF8TBT-b-P3HT. *Macromolecules* **2012**, *45* (10), 4142−4151.
(90) Jiang, Y.; Chen, J. Z. Y. Influence of Chain Rigidity on the Phase Behavior of Wormlike Diblock Copolymers. *Phys. Rev. Lett.* **2013**, *110* (13), 138305.
(91) Zhang, W.; Gomez, E. D.; Milner, S. T. Surface-Induced Chain Alignment of Semiflexible Polymers. *Macromolecules* **2016**, *49* (3), 963−971.